

# Penalized Least-Squares Dynamic Pinhole SPECT Image Reconstruction using a Smooth 4-D Image Prior and Multiresolution Spatiotemporal B-Splines

Bryan W. Reutter, *Senior Member, IEEE*, Rostyslav Boutchko, *Member, IEEE*,  
Ronald H. Huesman, *Fellow, IEEE*, Anne C. Sauve, and Grant T. Gullberg, *Fellow, IEEE*

## I. INTRODUCTION

**T**HE goal of this work is to quantitatively compare fatty acid metabolism in the hearts of Wistar-Kyoto (WKY) normal rats and spontaneously hypertensive rats (SHR) as a function of age, and thereby track physiological changes associated with the onset and progression of heart failure in the SHR model. The fatty acid analog,  $^{123}\text{I}$ -labeled BMIPP, was used in longitudinal metabolic imaging studies performed every seven months. Slow rotation of the SPECT camera necessitated modeling the radiotracer time variation in the tomographic image reconstruction algorithm, which yielded time-activity curve estimates for the blood and myocardium directly from dynamic projection data.

This work builds on our previous work in fully 4-D multiresolution SPECT image reconstruction [1], [2]. In the work presented here, a smooth 4-D image prior is used to obtain less-noisy, least-squares estimates of time-activity curves directly from projections for dynamic pinhole SPECT studies of  $^{123}\text{I}$ -BMIPP in the myocardium of two WKY normal rats and two SHRs. Compartmental modeling is then applied to the time-activity curves to obtain quantitative estimates of the metabolic rate of  $^{123}\text{I}$ -BMIPP in the myocardium. Results are presented for studies performed when the rats were age 7, 14, and 21 months.

This fully 4-D image reconstruction method can also be applied to dynamic PET.

## II. METHODS

### A. Penalized Least-Squares Reconstruction with a Smooth 4-D Image Prior

A dynamic SPECT projection data model that relates detected events to a 4-D spatiotemporal B-spline representation of a time-varying radiotracer distribution can be written as

$$\mathbf{p} = \mathbf{F}\mathbf{a}, \quad (1)$$

where  $\mathbf{p}$  is an  $I$ -element column vector of modeled dynamic projection data values,  $\mathbf{F}$  is an  $I \times M$  system matrix,  $\mathbf{a}$  is an  $M$ -element column vector of B-spline coefficients,  $I$  is

This work was supported by the National Institutes of Health of the U. S. Department of Health and Human Services under grants R01-EB00121, R01-EB007219, and R01-HL71253; and by the Director, Office of Science, Office of Biological and Environmental Research of the U. S. Department of Energy under contract DE-AC02-05CH11231.

B. W. Reutter, R. Boutchko, R. H. Huesman, A. C. Sauve, and G. T. Gullberg are with the Department of Radiotracer Development & Imaging Technology, Lawrence Berkeley National Laboratory, One Cyclotron Road, Berkeley, CA 94720, USA (e-mail: bwreutter@lbl.gov).

the total number of projection measurements acquired by the SPECT detector(s), and  $M$  is the number of 4-D B-spline basis functions that span the space and time to be reconstructed. The system matrix  $\mathbf{F}$  incorporates the spline model for time variation of the radiotracer distribution, as well as physical effects such as attenuation, depth-dependent collimator response, and scatter that affect detection of gamma rays emitted by the radiotracer distribution.

At the outset, the least-squares criterion to be minimized,  $\chi^2$ , is simply the sum of squared differences between the measured projections,  $\mathbf{p}^*$ , and the modeled projections:

$$\chi^2 = (\mathbf{p}^* - \mathbf{F}\mathbf{a})^T(\mathbf{p}^* - \mathbf{F}\mathbf{a}), \quad (2)$$

where the superscript “T” denotes the matrix transpose. Minimizing the criterion  $\chi^2$  yields an estimate,  $\hat{\mathbf{a}}$ , of coefficients for the 4-D B-spline basis functions that represent the time-varying radiotracer distribution:

$$\hat{\mathbf{a}} = (\mathbf{F}^T\mathbf{F})^{-1}\mathbf{F}^T\mathbf{p}^*. \quad (3)$$

The corresponding minimum value for the criterion  $\chi^2$  is

$$\chi_{\min}^2 = (\mathbf{p}^* - \mathbf{F}\hat{\mathbf{a}})^T(\mathbf{p}^* - \mathbf{F}\hat{\mathbf{a}}). \quad (4)$$

To reduce noise, we now wish to add a penalty term to the criterion  $\chi^2$  that encourages the reconstructed image to be smooth in both space and time. Insight into what a reasonable penalty term might be can be obtained by expressing  $\chi^2$  in terms of its minimum value:<sup>1</sup>

$$\begin{aligned} \chi^2 &= (\mathbf{p}^* - \mathbf{F}\mathbf{a})^T(\mathbf{p}^* - \mathbf{F}\mathbf{a}) \\ &= [(\mathbf{p}^* - \mathbf{F}\hat{\mathbf{a}}) - \mathbf{F}(\mathbf{a} - \hat{\mathbf{a}})]^T[(\mathbf{p}^* - \mathbf{F}\hat{\mathbf{a}}) - \mathbf{F}(\mathbf{a} - \hat{\mathbf{a}})] \\ &= \chi_{\min}^2 - 2(\mathbf{p}^* - \mathbf{F}\hat{\mathbf{a}})^T\mathbf{F}(\mathbf{a} - \hat{\mathbf{a}}) + (\mathbf{a} - \hat{\mathbf{a}})^T\mathbf{F}^T\mathbf{F}(\mathbf{a} - \hat{\mathbf{a}}) \\ &= \chi_{\min}^2 + (\mathbf{a} - \hat{\mathbf{a}})^T\mathbf{F}^T\mathbf{F}(\mathbf{a} - \hat{\mathbf{a}}). \end{aligned} \quad (5)$$

Inspecting (5), one sees that differences from the least-squares solution  $\hat{\mathbf{a}}$  are penalized by the term  $(\mathbf{a} - \hat{\mathbf{a}})^T\mathbf{F}^T\mathbf{F}(\mathbf{a} - \hat{\mathbf{a}})$ .

To mimic this effect for purposes of reducing noise, we propose to add a penalty term that resembles  $(\mathbf{a} - \boldsymbol{\alpha})^T\mathbf{F}^T\mathbf{F}(\mathbf{a} - \boldsymbol{\alpha})$ , where  $\boldsymbol{\alpha}$  is a smooth 4-D image prior obtained by normalizing a simple backprojection of the measured projections:

$$\boldsymbol{\alpha} = (\mathbf{F}^T\mathbf{p}^*) ./ (\mathbf{F}^T\mathbf{F}[1]), \quad (6)$$

where the operator “./” denotes pointwise division of elements in the left operand by the corresponding elements in the

<sup>1</sup>The term that is linear with respect to  $(\mathbf{a} - \hat{\mathbf{a}})$  vanishes because the model error  $\mathbf{p}^* - \mathbf{F}\hat{\mathbf{a}}$  lies in the null space of the backprojection operator  $\mathbf{F}^T$ .

right operand and “[1]” denotes an  $M$ -element column vector of ones.<sup>2</sup> Note that the image prior  $\alpha$  has the desirable physiologic property of being nonnegative—thus, the reconstructed image is encouraged to have nonnegative 4-D B-spline coefficients.

The penalty term that we propose to use is

$$\sum_{i=1}^I \sum_{m=1}^M [F_{im}(a_m - \alpha_m)]^2, \quad (7)$$

where  $F_{im}$  is the  $(i, m)$ -th element of the system matrix  $\mathbf{F}$ ,  $a_m$  is the  $m$ -th element of the spline coefficient vector  $\mathbf{a}$ , and  $\alpha_m$  is the  $m$ -th element of the smooth image prior  $\alpha$ . For the resulting negatively correlated, zero-mean elements in the vector  $(\mathbf{a} - \alpha)$ , (7) imposes a penalty that is greater than the penalty imposed by  $(\mathbf{a} - \alpha)^T \mathbf{F}^T \mathbf{F} (\mathbf{a} - \alpha)$ . The latter penalty can be expressed as<sup>3</sup>

$$\sum_{i=1}^I \left[ \sum_{m=1}^M F_{im}(a_m - \alpha_m) \right]^2. \quad (8)$$

### B. Pinhole SPECT Data Acquisition and System Modeling

With use of methods described in [3], dynamic cardiac pinhole SPECT projection data and pinhole geometric calibration data were acquired on a dual-head GE Millennium VG Hawkeye SPECT/CT scanner equipped with custom pinhole collimators (Fig. 1). For each study, an injection of about 4 mCi of  $^{123}\text{I}$ -BMIPP was performed shortly after the dynamic data acquisition began. Data were acquired for 60 min in 1-sec time frames with an angular step of 4 degrees per frame. Collimator response was modeled via ray tracing and excluded the effects of collimator penetration. The system model also excluded the effects of attenuation and scatter; however, we are currently studying these effects via Monte Carlo simulation in a separate investigation [4], [5].

### C. Fully 3-D Late Static Image Reconstruction

To determine spatial locations for the left ventricular blood pool and myocardial tissue, late data acquired 1.5–60 min after injection were summed and a static image was reconstructed with use of a 3-D version of the penalized least-squares algorithm presented here. The late static spatial distribution of  $^{123}\text{I}$ -BMIPP was modeled with use of 3-D multiresolution spatial B-splines that were piecewise constant. The 3-D spatial splines were organized on a  $20 \times 20 \times 20$  3-D grid that provided uniform sampling of 3.2 mm in each dimension. Inside the volume containing the heart, a  $6 \times 6 \times 6$  neighborhood of these lower-resolution splines was replaced by a  $12 \times 12 \times 12$  neighborhood of higher-resolution splines that provided uniform sampling of 1.6 mm.

<sup>2</sup>Normalization by  $\mathbf{F}^T \mathbf{F} [1]$  ensures that backprojecting the noiseless projections of a constant image yields the original constant image.

<sup>3</sup>In general, the penalties (7) or (8) may be scaled by a smoothing parameter  $\beta$ . By virtue of (5), a reasonable value is  $\beta = 1$ , which was used for the work presented here.



Fig. 1. Clinical dual-head SPECT/CT scanner with custom pinhole collimators used for quantitative dynamic imaging of fatty acid metabolism in the rat heart.

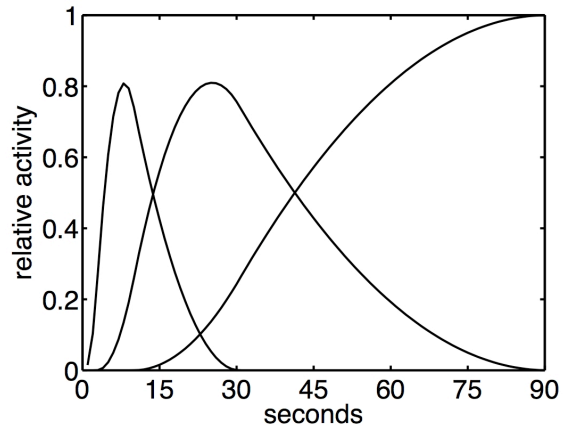


Fig. 2. Piecewise quadratic temporal B-spline basis functions used to reconstruct dynamic data from the first gantry rotation.

### D. Fully 4-D Early Dynamic Image Reconstruction

To quantify fatty acid metabolism in the rat heart, early data acquired 0–1.5 min after injection were not summed and a dynamic image was reconstructed with use of the 4-D penalized least-squares algorithm presented here. The time-varying spatial distribution of  $^{123}\text{I}$ -BMIPP was modeled with use of 4-D multiresolution B-splines that were piecewise constant in space and piecewise quadratic in time. The 4-D splines were spatially organized on a  $10 \times 10 \times 10$  3-D grid that provided uniform sampling of 6.4 mm in each dimension. Inside the volume containing the heart, a  $3 \times 3 \times 3$  neighborhood of these lower-resolution splines was replaced by a  $12 \times 12 \times 12$  neighborhood of higher-resolution splines that provided uniform sampling of 1.6 mm. The 4-D splines were temporally organized on a 1-D grid that provided nonuniform sampling intervals of 0–2.4, 2.4–9.4, 9.4–30, and 30–90 sec during the first gantry rotation (Fig. 2).

### E. Compartmental Modeling of Fatty Acid Metabolism

Left ventricular blood pool and myocardial tissue locations were identified in the late 3-D static image, and time-activity curves were obtained by sampling the early 4-D dynamic image at these locations. A one-tissue-compartment model (Fig. 3) was then fitted to the time-activity curves to obtain a quantitative estimate of the metabolic rate of  $^{123}\text{I}$ -BMIPP

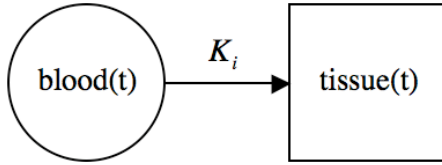


Fig. 3. One-tissue-compartment model used for quantifying fatty acid metabolism during the first 1.5 min after injection of  $^{123}\text{I}$ -BMIPP.

in the rat myocardium. Early myocardial tissue uptake was modeled with a single, irreversible compartment:

$$\text{tissue}(t) = K_i \cdot \int_0^t \text{blood}(\tau) d\tau, \quad (9)$$

where  $K_i$  is the metabolic rate of  $^{123}\text{I}$ -BMIPP. Myocardial tissue voxels were modeled as mixture of blood input and tissue uptake:

$$\text{voxel}(t) = [f_v \cdot \text{blood}(t)] + \left[ K_i \cdot \int_0^t \text{blood}(\tau) d\tau \right], \quad (10)$$

where  $f_v$  is the fraction of vasculature in the tissue and also incorporates the effect of spillover from the blood pool to the tissue.

### III. RESULTS

In the late 3-D static images (Fig. 4, next page), more trapping of  $^{123}\text{I}$ -BMIPP is evident in the WKY normal hearts, compared to the SHR hearts.

For the early 4-D dynamic images, the use of nonuniform time sampling with splines that varied quadratically in time yielded smooth time-activity curves (Fig. 5, next page) that captured the relatively fast rise and fall of  $^{123}\text{I}$ -BMIPP in the left ventricular blood pool, as well as the uptake and initial trapping of the radiotracer in the left ventricular myocardium.

From these time-activity curves, compartmental modeling yielded estimates of  $K_i$  shown in Fig. 6 (this page). The decline with age of the rate of fatty acid metabolism in the heart is what one expects. The generally slower rates of fatty acid metabolism in the SHRs, compared to the WKY normal rats, is also what one expects as the SHR hearts switch to a reliance on glycolysis as the primary pathway for energy production during the development of heart failure.

### IV. DISCUSSION

This analysis method enables quantitative dynamic imaging of fatty acid metabolism in the rat heart, even with slow camera rotation. To the best of our knowledge, no other group has successfully developed a method to reconstruct the blood input function from small animal dynamic pinhole SPECT data acquired with slow camera rotation.

Future work includes correcting for spillover from tissue to the blood pool. Future work also includes addressing computational issues associated with reconstructing a dynamic image from the entire 60 min of projection data. It is anticipated that an additional, reversible tissue compartment will need to be

added to the compartmental model to account for washout of  $^{123}\text{I}$ -BMIPP from the myocardium over this longer time scale.

This fully 4-D image reconstruction method can also be applied to dynamic PET.

### ACKNOWLEDGMENT

This work was supported by the National Institutes of Health of the U. S. Department of Health and Human Services under grants R01-EB00121, R01-EB007219, and R01-HL71253; and by the Director, Office of Science, Office of Biological and Environmental Research of the U. S. Department of Energy under contract DE-AC02-05CH11231.

### REFERENCES

- [1] B. W. Reutter, G. T. Gullberg, R. Boutchko, K. Balakrishnan, E. H. Botvinick, and R. H. Huesman, "Fully 4-D dynamic cardiac SPECT image reconstruction using spatiotemporal B-spline voxelization," in *2007 IEEE Nuclear Science Symposium and Medical Imaging Conference Record*, B. Yu, Ed., 2007, pp. 4217–4221.
- [2] B. W. Reutter, R. Boutchko, R. H. Huesman, S. M. Hanrahan, K. M. Brennan, A. C. Sauve, and G. T. Gullberg, "Dynamic pinhole SPECT imaging and compartmental modeling of fatty acid metabolism in the rat heart," in *2008 IEEE Nuclear Science Symposium and Medical Imaging Conference Record*, P. Sellin, Ed., 2008, pp. 4478–4481.
- [3] J. Hu, A. Sitek, B. W. Reutter, R. H. Huesman, and G. T. Gullberg, "A new approach of dynamic pinhole SPECT imaging for evaluation of sympathetic nervous system function in animal models of cardiac hypertrophy," in *2005 IEEE Nuclear Science Symposium and Medical Imaging Conference Record*, B. Yu, Ed., 2005, pp. 2542–2546.
- [4] A. Sauve, W. Choong, R. Boutchko, B. W. Reutter, A. Hwang, E. W. Izaguirre, B. H. Hasegawa, and G. T. Gullberg, "Quantitative imaging of cardiovascular function with pinhole SPECT in mice and rats — effects of attenuation and scatter," *J Nucl Med*, vol. 48, no. 5 suppl, pp. 424P–425P, 2007 (abstract).
- [5] A. C. Sauve, B. W. Reutter, R. Boutchko, W.-S. Choong, R. H. Huesman, and G. T. Gullberg, "Multi-slice SPECT attenuation and scatter correction using Monte Carlo simulated system matrices," in *2008 IEEE Nuclear Science Symposium and Medical Imaging Conference Record*, P. Sellin, Ed., 2008, pp. 4273–4276.

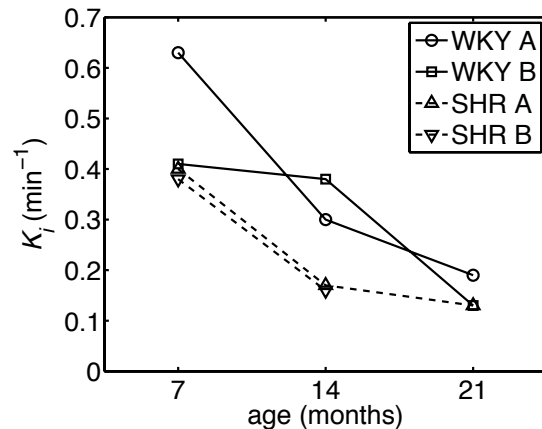


Fig. 6. Metabolic rate of  $^{123}\text{I}$ -BMIPP in the myocardium as a function of age.

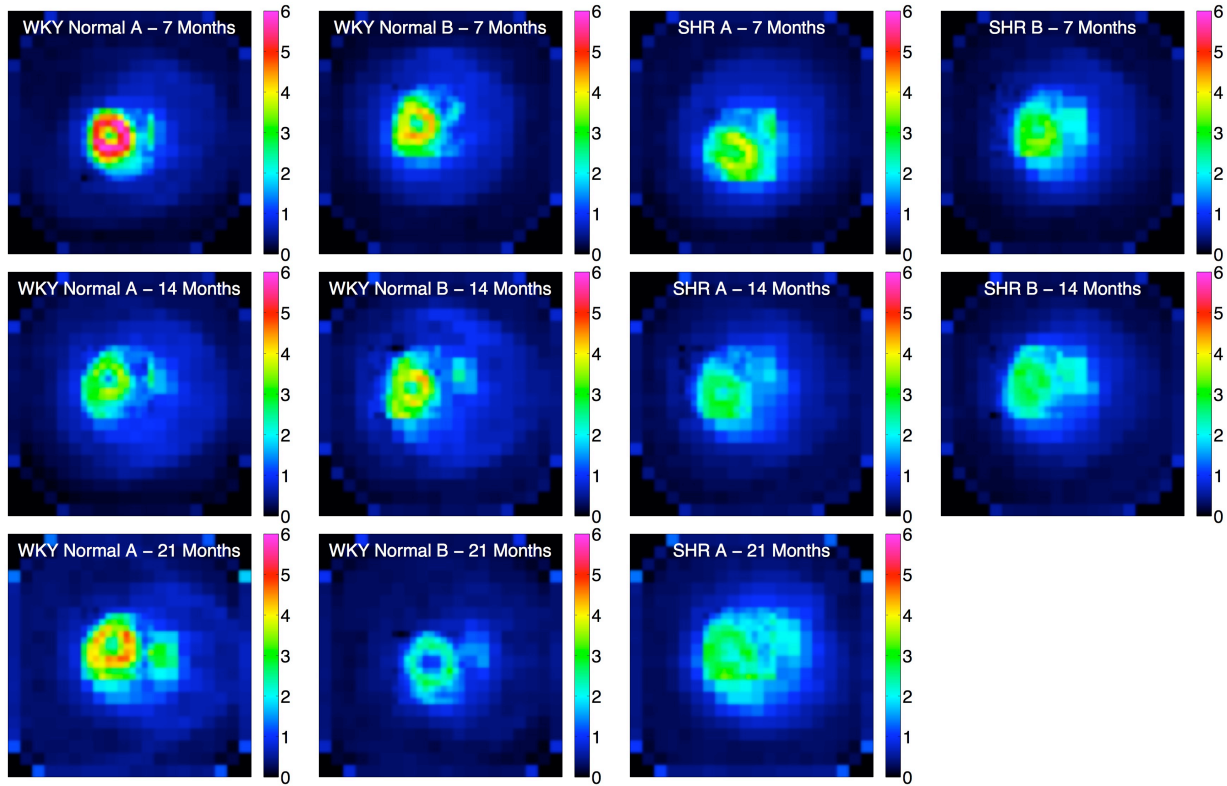


Fig. 4. Typically, more trapping of  $^{123}\text{I}$ -BMIPP is evident in late 3-D static images of the WKY normal hearts (left two columns), compared to the SHR hearts (right two columns). Trapping also tends to decrease with age (top row, 7 months; middle row, 14 months; bottom row, 21 months). SHR B died of congestive heart failure before 21 months.

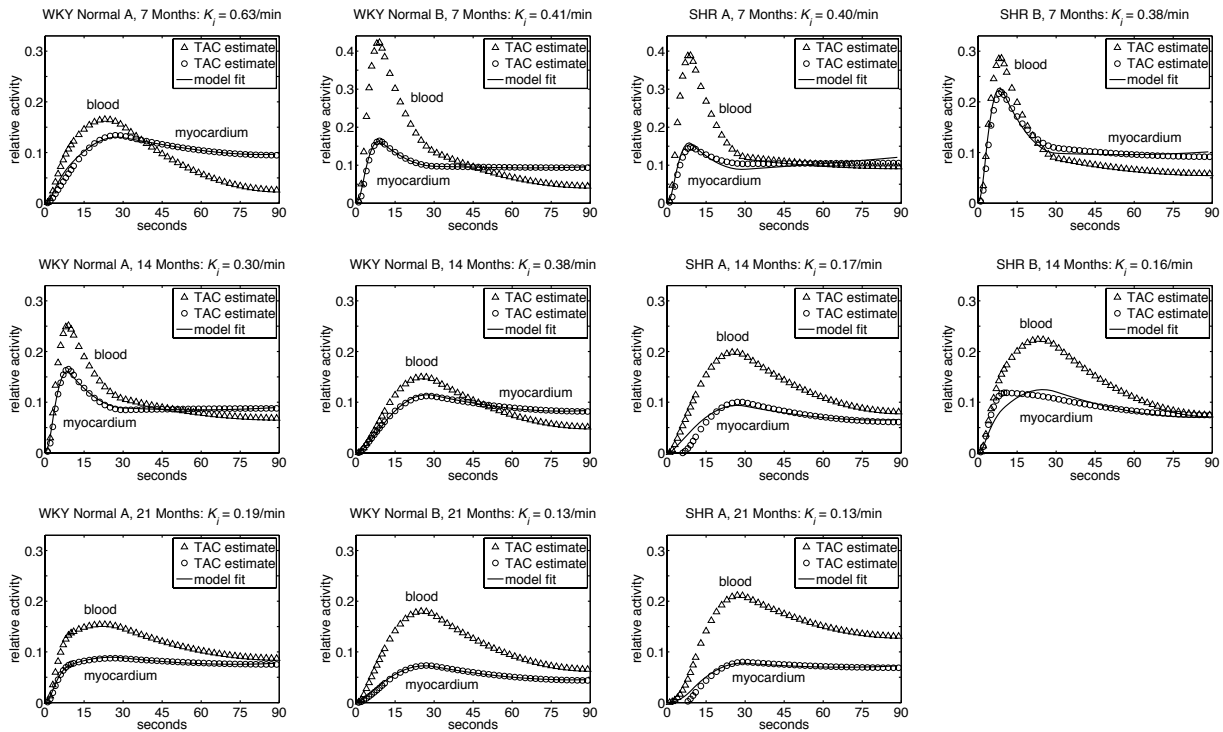


Fig. 5. Time-activity curves for the WKY normal rats (left two columns) and the SHRs (right two columns) capture quantitative differences between their blood inputs and myocardial uptakes (triangles and circles, respectively). Compartmental models (solid lines) provide good fits to the myocardial uptake curves. Top row, 7 months; middle row, 14 months; bottom row, 21 months. SHR B died of congestive heart failure before 21 months.